Bioactive Materials 40 (2024) 624–633

Contents lists available at ScienceDirect

Bioactive Materials

journal homepage: www.keaipublishing.com/en/journals/bioactive-materials

Promoting chondrogenesis by targeted delivery to the degenerating cartilage in early treatment of osteoarthritis

Yuxiang Fei [a,b,c,1], Xiaojing Li [d,1], Zhongyang Lv [e,1], Zizheng Liu [a,b,c], Ya Xie [a,b,c], Jiaqi Chen [a,b,c], Weitong Li [a,b,c], Xiyu Liu [a,b,c], Hu Guo [a,b,c], Huan Liu [a,b,c], Zhaofeng Zhang [a,b,c], Xunhao Wang [a,b,c], Jingjing Fan [a,b,c], Chunqing Hu [a,b,c], Xiaoyu Jin [a,b,c], Ruiyang Jiang [a,b,c], Nuo Xu [a,b,c], Jiang Xia [f], Yang Li [d,**], Dongquan Shi [a,b,c,*]

[a] Division of Sports Medicine and Adult Reconstructive Surgery, Department of Orthopedic Surgery, Nanjing Drum Tower Hospital, Affiliated Hospital of Medical School, Nanjing University, 321 Zhongshan Road, Nanjing, 210008, Jiangsu, PR China
[b] State Key Laboratory of Pharmaceutical Biotechnology, Nanjing University, Nanjing, Jiangsu, PR China
[c] Branch of National Clinical Research Center for Orthopedics, Sports Medicine and Rehabilitation, PR China
[d] Guangdong Provincial Engineering Research Center of Molecular Imaging, Guangdong-Hong Kong-Macao University Joint Laboratory of Interventional Medicine, The Fifth Affiliated Hospital, Sun Yat-sen University, Zhuhai, 519000, Guangdong, PR China
[e] Department of Orthopedics, Nanjing Jinling Hospital, Affiliated Hospital of Medical School, Nanjing University, Nanjing, 210002, PR China
[f] Department of Chemistry, The Chinese University of Hong Kong, Shatin, Hong Kong SAR China

ARTICLE INFO

Keywords:
Early-stage osteoarthritis
Targeting therapy
Collagen
Triple helix
Albumin nanoparticle

ABSTRACT

Osteoarthritis (OA) is a highly incident total joint degenerative disease with cartilage degeneration as the primary pathogenesis. The cartilage matrix is mainly composed of collagen, a matrix protein with a hallmark triple-helix structure, which unfolds with collagen degradation on the cartilage surface. A collagen hybridizing peptide (CHP) is a synthetic peptide that binds the denatured collagen triple helix, conferring a potential disease-targeting possibility for early-stage OA. Here, we constructed an albumin nanoparticle (An) conjugated with CHP, loaded with a chondrogenesis-promoting small molecule drug, kartogenin (KGN). The CHP-KGN-An particle exhibited sustained release of KGN in vitro and prolonged in vivo retention selectively within the degenerated cartilage in the knee joints of model mice with early-stage OA. Compared to treatment with KGN alone, CHP-KGN-An robustly attenuated cartilage degradation, synovitis, osteophyte formation, and subchondral bone sclerosis in OA model mice and exhibited a more prominent effect on physical activity improvement and pain alleviation. Our study showcases that targeting the degenerated cartilage by collagen hybridization can remarkably promote the efficacy of small molecule drugs and may provide a novel delivery strategy for early-stage OA therapeutics.

Peer review under responsibility of KeAi Communications Co., Ltd.

* Corresponding authors. State Key Laboratory of Pharmaceutical Biotechnology, Division of Sports Medicine and Adult Reconstructive Surgery, Department of Orthopedic Surgery, Nanjing Drum Tower Hospital, The Affiliated Hospital of Nanjing University Medical School, 321 Zhongshan Road, Nanjing, 210008, Jiangsu, PR China.

** Corresponding author. Guangdong Provincial Engineering Research Center of Molecular Imaging, Guangdong-Hong Kong-Macao University Joint Laboratory of Interventional Medicine, The Fifth Affiliated Hospital, Sun Yat-sen University, 52 Meihua Road, Zhuhai, 519000, Guangdong, PR China.

E-mail addresses: 975778674@qq.com (Y. Fei), lixj273@mail2.sysu.edu.cn (X. Li), zhongyanglv@163.com (Z. Lv), liuzizheng2020@163.com (Z. Liu), 459895571@qq.com (Y. Xie), 2250317381@qq.com (J. Chen), 1554845347@qq.com (W. Li), liuxiyu1992@live.com (X. Liu), 15050583626@163.com (H. Guo), lhhuan0104@163.com (H. Liu), 18330586115@163.com (Z. Zhang), drfrank123@163.com (X. Wang), fanjingjing0730@163.com (J. Fan), 2042325296@qq.com (C. Hu), 1152123889@qq.com (X. Jin), jry1028@163.com (R. Jiang), Xxxnisok@163.com (N. Xu), jiangxia@cuhk.edu.hk (J. Xia), liyang266@mail.sysu.edu.cn (Y. Li), shidongquan@nju.edu.cn (D. Shi).

[1] Yuxiang Fei, Xiaojing Li, and Zhongyang Lv contributed equally to this work.

https://doi.org/10.1016/j.bioactmat.2024.08.004
Received 8 April 2024; Received in revised form 21 July 2024; Accepted 6 August 2024

1. Introduction

Osteoarthritis (OA) is a pervasive degenerative joint disease characterized by cartilage degeneration, synovitis, and periarticular bone remodeling [1]. With disease aggravation, these pathological changes bring unbearable pain and joint dysfunction, and more severely, lead to disability [1]. Early-stage OA is regarded as a window of opportunity for therapeutic intervention when the cartilage degeneration is difficult to macroscopically detect and regeneration is less challenging [2]. However, to date, no specific therapeutic strategy has been clinically exploited for early-stage OA [2,3]. The clinical OA treatments are mainly symptom-oriented, which are ineffective in stopping the disease development [4]. Therefore, effective and accurate chondrogenic therapies suitable for early-stage OA are urgently pursued by clinicians [2].

One major obstacle to developing disease-modifying therapeutics for OA is the difficulty of delivering them to the dense and avascular cartilage tissue [5–8]. Therefore, drug carriers that respond to the pathological factors in the OA tissue microenvironment including reactive oxygen species [9], matrix metalloproteinases (MMPs) [10], and low pH [11], or directly adhere to the cartilage matrix [e.g., cartilage-targeting peptides [12], collagen II antibodies [13], and chondrocyte-membrane coating [5] have been vigorously developed. However, efforts of therapeutic delivery that directly target the diseased cartilage are surprisingly lacking, even though cartilage degeneration is a defining pathological feature of OA progression [14,15]. Considering the abundance of healthy cartilage in early-stage OA, such a delivery approach shall promote treatment efficacy and reduce unexpected adverse effects on normal cartilage by further concentrating the therapeutics on the disease-affected degenerating tissue.

Collagen is the predominant component of the articular cartilage matrix, and its molecule possesses a hallmark triple-helical folding. We envision that during cartilage degeneration, the collagen molecule may be damaged, leaving its triple helix structure unfolded [16,17]. We also speculate that disruption to the collagen triple helix may occur during early-stage OA, preceding the progressing stage when cartilage degeneration becomes observable histologically. Previously, we and others developed the collagen hybridizing peptide (CHP), a synthetic peptide consisting of repeating triplets of glycine, proline, and hydroxyproline [18], which specifically binds the damaged, but not intact collagen matrices by reforming a triple helix with the unfolded collagen chains [19–21]. We recently demonstrated its capability to target the degenerating cartilage and other osteoarthritic joint tissues in mice when histological and radiological changes are insignificant [22]. This unique property makes CHP an effective vehicle for targeted delivery of chondrogenic therapy to cartilage tissue with only subtle erosion in early-stage OA.

Kartogenin (KGN) is a small-molecule compound known to promote stem cell differentiation into chondrocytes, help chondrocytes resist inflammation, and alleviate OA symptoms [23,24]. However, it has low water solubility and is easily cleared by the rapidly renewing synovial fluid within the joint [25]. Additionally, its potential to stimulate abnormal proliferation in healthy tissues limits its direct in vivo applications without a disease-targeting delivery platform [26–28]. Here, we present a chondrogenic agent, comprising a KGN-encapsulated albumin nanoparticle functionalized with CHP, and demonstrate its enhanced efficacy in treating early-stage OA in a mouse model by targeted delivery to the degenerated cartilage.

2. Results and discussion

2.1. CHP conjugation with KGN-encapsulated albumin particles

We selected albumin nanoparticles to deliver KGN because they are often used in clinical formulations to carry hydrophobic small-molecule compounds, such as paclitaxel [29]. We formulated the bovine albumin nanoparticles with KGN-encapsulation using a desolvation method modified from Jahanban-Esfahlan et al. [30], followed by covalent modification with a DBCO-sulfo-NHS ester for subsequent conjugation with an azide-functionalized CHP moiety through copper-free click reaction (Fig. 1a, see Methods for details). The same protocol was also used to prepare nanoparticles without CHP functionalization (KGN-An) or KGN-encapsulation (CHP-An) and a nanoparticle conjugated with a fluorescently labeled Cy5-CHP (Cy5-CHP-KGN-An). The high-concentration suspension of the final non-fluorescent particle products exhibited a milky white translucent appearance (Fig. 1b). The clinical application of KGN is hindered by its extremely low water solubility (< 0.1 mg/mL) [31] which was increased by over an order of magnitude to nearly 1 mg/mL in our hands via albumin encapsulation. By using a formulation of CHP: KGN: albumin in 3:10:1 (molar ratio), the encapsulation efficiency of KGN reached 67 %. These albumin particles, with or without the conjugation of a short CHP peptide (estimated length: < 10 nm) [32] all exhibited a homogeneous size distribution between 100 and 200 nm under dynamic light scattering (DLS) measurements (Fig. 1b) and scanning electron microscopy (SEM) observation (Fig. 1c). Since albumin is rich in negatively charged amino acid residues, these particles all possessed a negative zeta potential (-22∼-34 mV, Fig. 1d), which prevents aggregation and contributes to their stability in storage. Moreover, because native cartilage possesses strong negative charges [33], these albumin particles are expected to be electrostatically repelled from the cartilage tissue, reducing their non-specific binding and uptake in the healthy joint. Finally, as the aggregated, crosslinked albumin macromolecules gradually disassemble or degrade, the physically bound KGN is released from the nanocarriers [34]. Our in vitro testing showed that albumin encapsulation could sustain the KGN release into the PBS solution for over 7 days, and this release efficiency was not affected after the modification of the CHP peptide (Fig. 1e).

2.2. Targeted retention of CHP-KGN-An in degenerated cartilage in a mouse model of early-stage OA

We tested whether the CHP peptide, as a targeting moiety, could promote the delivery of the KGN-loaded nanoparticle to the damaged cartilage in an OA mouse model (12-week-old C57BL/6 mice) induced by destabilization of the medial meniscus (DMM) in the right knee (with a sham operation in the left knee). The delivery and treatment were tested in mice 4 weeks post-operation when immunohistochemical (IHC) staining of the cartilage showed no significant defects and no difference in the Col II^{+} area between DMM and sham-operated knees (Supplementary Fig. 1). The mice systemically administered (tail-vein injection) with Cy5-labeled CHP-KGN-An consistently showed more prominent Cy5 fluorescence in the DMM-injured knees than that of the sham-operated knees, when imaged in vivo and ex vivo with an IVIS fluorescence imager [5 h post-injection (p.i.)] (Fig. 2a). Subsequently, the mice were intra-articularly injected with the Cy5-labeled CHP-KGN-An 5 h before harvesting the knee cartilage tissue for histologic analysis. Fluorescence imaging of the joint cryosections showed pronounced uptake of the in vivo administered Cy5-CHP-KGN-An into the transitional and deep zones of the cartilage from the DMM- but not the sham-operated knees (Fig. 2b). Meanwhile, Cy5-^{S}CHP-KGN-An, a control nanoparticle functionalized with a scrambled CHP sequence without the collagen hybridizing capacity [35], exhibited only low non-specific binding without cartilage enrichment in the joint tissues (Fig. 2b), when it was administered and analyzed in the same fashion. These data demonstrated that the CHP-KGN-An vehicle can target the degenerated cartilage in vivo in an early-stage osteoarthritic mouse model through CHP's specific binding to the denatured collagen molecules.

We further evaluated the in vivo retention of the intra-articularly administered Cy5-CHP-KGN-An in the DMM- and sham-operated knee joints by daily live IVIS imaging and quantification of the fluorescence signals in the knee joint areas. A greater retention of the KGN-delivering particles was found in the DMM-operated knee than in the sham-

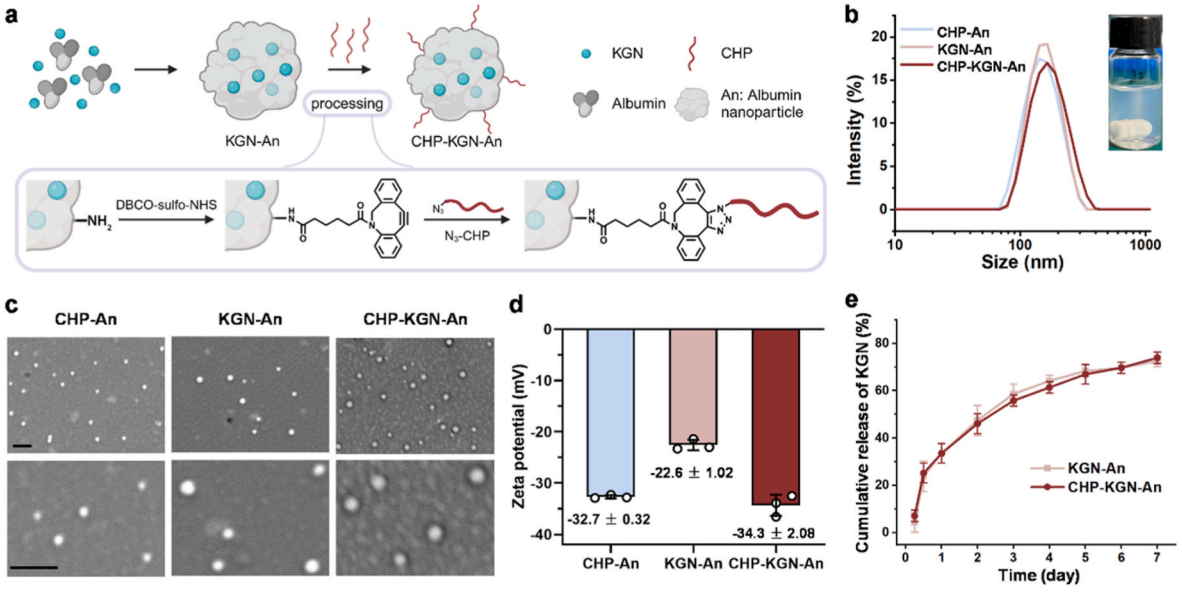

Fig. 1. Preparation and characterization of the CHP-functionalized and KGN-encapsulated albumin particles (CHP-KGN-An) as a drug-delivery vehicle. (a) Schematic of the conjugation of CHP to KGN-An using a copper-free click reaction. (b) Size distribution of nanoparticles CHP-An, KGN-An, and CHP-KGN-An measured by DLS. (c) SEM images of nanoparticles CHP-An, KGN-An, and CHP-KGN-An. Scale bars, 1000 nm. (d) Zeta potentials of nanoparticles CHP-An, KGN-An, and CHP-KGN-An. Data are shown as mean ± SD. (e) The release profile of KGN from KGN-An and CHP-KGN-An in PBS over 7 days (n = 3 independent experiments; data shown as mean ± SD).

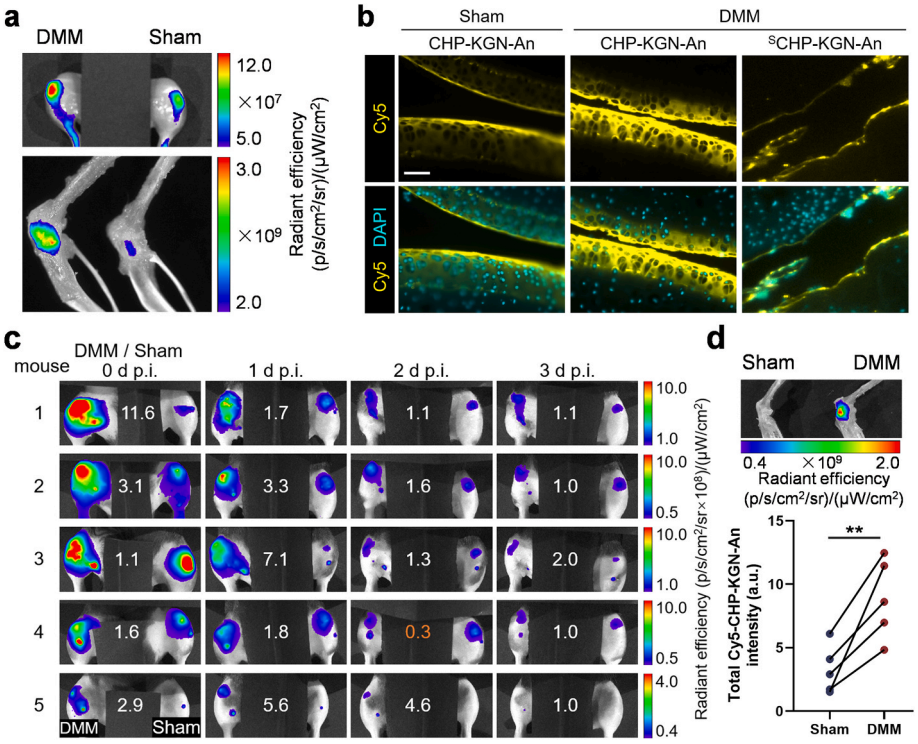

Fig. 2. In vivo targeted retention of CHP-KGN-An in the degenerated cartilage. (a) Representative ex vivo fluorescence images of knee joints 5 h post-tail-vein injection of Cy5-CHP-KGN-An in mice 4 weeks post-DMM-operation (n = 5 mice). (b) Representative fluorescent images of the cryosections of knee joint cartilage taken 5 h following intra-articular injection in mice. (c) Daily in vivo fluorescence images showing Cy5-CHP-KGN-An's retention in the knee joints of the mice following an intra-articular injection on day 0 (1 h p.i., n = 5 mice). The ratio between the fluorescence signals quantified from each mouse's DMM- and sham-operated knee area is displayed for each image with the only ratio lower than 1 shown in brown. (d) Post-mortal measurements of the paired fluorescence signals from the isolated knee joint specimens on day 4 post-injection with a representative fluorescence image (n = 5 mice). Different imaging parameters were used for the ex vivo and in vivo fluorescence images. Data are analyzed with a paired *t*-test. $^{**}P < 0.01$.

operated one for days in each mouse we tested (Fig. 2c). Although the signal difference between the DMM- and sham-operated knees seemed deminished 3 d p.i., post-mortal measurements of the fluorescence from the isolated knee joint specimens 4 d p.i. showed consistently stronger Cy5-CHP-KGN-An retention in the DMM-knee than the paired sham-knee in individual mice (Fig. 2d). Additional fluorescence examinations suggested that the Cy5-CHP-KGN-An particles are mainly cleared and metabolized through the liver (Supplementary Fig. 2). These data suggested that CHP-KGN-An can be selectively uptaken and retained by the degenerated cartilage in the early-stage, rendering a sustained drug-releasing effect in vivo.

2.3. CHP-KGN-An improves the movement function of the DMM-operated joints in mice

After verifying the targeting ability of CHP-KGN-An to the degenerated cartilage, we evaluated its therapeutic effects in vivo. We injected saline (8 μL), KGN (50 μM, 8 μL), KGN-An (KGN 50 μM, 8 μL), CHP-KGN-

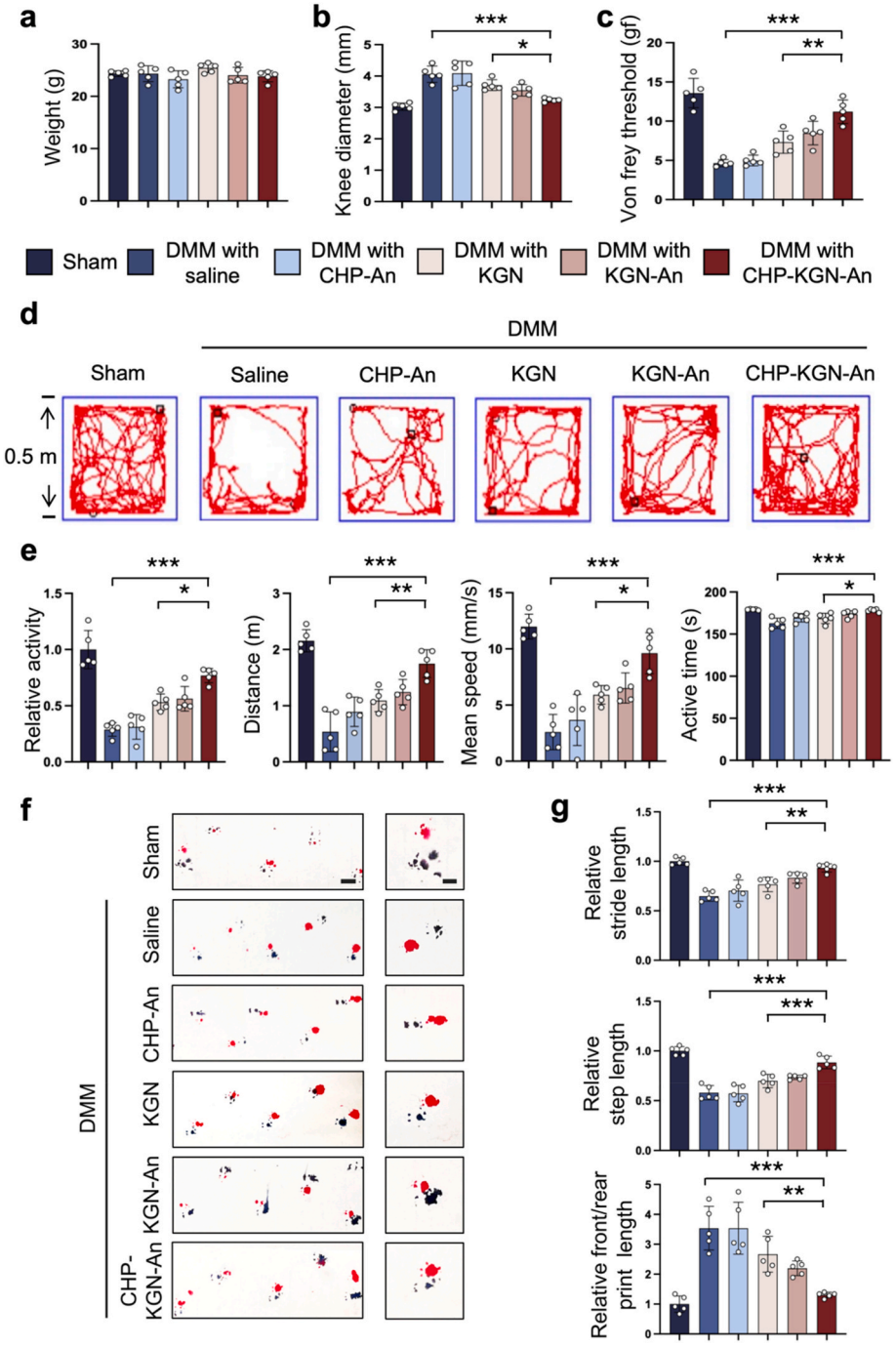

Fig. 3. CHP-KGN-An improved the therapeutic effect of KGN on the motion function of the DMM mice. (a) The weight of the mice in this study (n = 5 mice). (b) The knee diameter of mice treated as indicated. (c) The quantification of paw contract thresholds was measured with the Von Frey Fiber test. (d) Representative mice movement trajectories in the open field test. (e) The quantification of the relative activity, distance, mean speed, and active time in the open field test (n = 5). (f) Representative mouse footmarks in the footprint assay. Red footprints: forelimbs; black footprints: hind limbs. Scale bars, 1 cm (left), 5 mm (right). (g) The CHP-KGN-An treatment further increased the relative stride and step length and reduced the relative front/rear print length in the DMM mice compared to the KGN treatment group (n = 5). Data are shown as mean ± SD and analyzed using one-way ANOVA with Tukey's post-hoc test. *$P < 0.05$; **$P < 0.01$; ***$P < 0.001$.

An (KGN 50 μM, 8 μL) or CHP-An (using the same An concentration as CHP-KGN-An, 8 μL) into the DMM-operated joints of the mice weekly. Ten weeks after the surgery, the mice's body weight showed no difference for all groups (Fig. 3a). The mean diameter of the DMM knee joints treated with the CHP-KGN-An was lower than that of the untreated and the KGN-only groups, suggesting a reduction in joint swelling (Fig. 3b). The Von Frey Fiber test showed that the DMM injury significantly reduced the paw withdrawal response threshold in mice, indicating decreased pain tolerance (Fig. 3c). The pain tolerance was moderately improved with the KGN treatment but substantially more with the CHP-KGN-An treatment, suggesting an enhanced effect on knee pain alleviation by CHP-KGN-An (Fig. 3c). We then conducted the open field test (OFT), where 3 min of trajectories of the mice's free movements were recorded and analyzed to assess their motion ability (Fig. 3d). In the OFT, the relative activity level, total movement distance, active time, and mean speed all significantly increased with the CHP-KGN-An treatment from the level of the saline group, showing a much more robust effect than the KGN-only treatment (Fig. 3e). Furthermore, we conducted a footprint experiment to study the mice's gait changes (Fig. 3f). The tests showed that compared to the KGN-alone treatment, the CHP-KGN-An treatment further increased the step and stride length and reduced the front-rear footprint gap in the DMM-injured mice, suggesting its enhanced efficacy on hyperalgesia and joint stiffness (Fig. 3g) [36,37]. Overall, our findings from these activity studies indicate that the targeted delivery of CHP-KGN-An significantly improves the therapeutic effect of KGN on the motion functions of the DMM-injured joints in mice.

2.4. CHP-KGN-An enhances the protective effect of KGN against DMM-induced cartilage degeneration

After conducting the behavioral experiments, the mice were euthanized and the knee joints were surgical collected for paraffin-embedded sectioning and histological analysis. The chondrogenic effect of KGN and its regulation on the catabolic balance of chondrocytes have been well demonstrated and documented [23,24,38,39]. Our study aimed to enhance these therapeutic effects through CHP-KGN-An delivery. Safranin-O/fast green (S.O.) and toluidine blue staining showed that the cartilage of the DMM mice was severely damaged compared to the sham group (Fig. 4a and b). As expected, KGN alleviated cartilage damage in the DMM mice. Yet the CHP-KGN-An treatment group showed a thicker cartilage (Fig. 4c–f), an lower Osteoarthritis Research Society International (OARSI) score (Fig. 4d), and a higher chondrocyte number (Fig. 4e) compared to the KGN treatment group. Immunohistochemically, the CHP-KGN-An treatment group showed a higher expression of anabolic markers (Col II, Aggrecan, and Sox9) and a lower expression of catabolic markers (Mmp13 and Adamts5) compared to the KGN treatment group, indicating a lower degree of cartilage degradation (Fig. 4h–k and Supplementary Fig. 3). These data demonstrate that CHP-KGN-An enhances the protective effect of KGN on the ECM synthesis and degradation in the OA model mice's cartilage, thereby countering the progression of OA.

2.5. CHP-KGN-An alleviates osteophyte formation, subchondral bone remodeling, and synovitis in the DMM mice

Next, we quantified the osteophyte, subchondral bone thickness, and synovitis scores in the DMM mice with different treatments. Micro-computed tomography (micro-CT) scanning and further three-dimensional reconstruction (Fig. 5a) exhibited significant osteophyte formation and subchondral bone sclerosis in the DMM joints, indicating abnormal bone remodeling during OA progression (Fig. 5d and e). KGN treatment reduced the osteophyte quantity and subchondral bone thickness in the DMM mice, while a more robust effect was observed in the CHP-KGN-An treated group (Fig. 5d and e). Moreover, Hematoxylin & eosin (H&E) staining (Fig. 5b) showed that the CHP-KGN-An treatment group exhibited an even lower synovitis score (measured by inflammatory cell infiltration and synovial thickness) compared to the KGN treatment group (Fig. 5c). These findings indicated that CHP-KGN-An enhances the alleviating effects of KGN on bone remodeling and synovitis in the degenerating joints.

2.6. Biocompatibility of CHP-KGN-An

Lastly, we tested the biocompatibility of CHP-KGN-An. In a cell assay, we co-cultured KGN (5 μM) and CHP-KGN-An (releasing the same dose of KGN within 24 h) with chondrocytes. After 24 h, Calcein-AM/PI and phalloidin staining showed that chondrocytes treated with the same doses of KGN and CHP-KGN-An exhibited a survival rate and cytoskeleton morphology comparable to the untreated chondrocytes (Fig. 6a–c). We then co-cultured chondrocytes with KGN (from 100 nM to 5 μM) and CHP-KGN-An (releasing the equivalent doses of KGN within 72 h). CCK8 assays showed that neither KGN nor CHP-KGN-An significantly affect the chondrocyte viability within this concentration range (Fig. 6d, e and Supplementary Fig. 4). These results demonstrated the high biocompatibility of CHP-KGN-An to chondrocytes. Meanwhile, in an in vivo test, after euthanizing the mice, histological analysis showed no apparent morphological or cellular abnormality in their heart, liver, spleen, lung, or kidney (Fig. 6f). These data indicated the CHP-KGN-An's biocompatibility under the tested concentrations preliminarily.

3. Conclusion

We demonstrate that CHP-KGN-An delays OA progression by targeted delivering chondrogenic agents to deteriorating cartilage in mice. This study provides a promising therapeutic delivery approach for the precise treatment of early-stage OA.

4. Methods and materials

4.1. Preparation and in vitro characterization of CHP-KGN-an

KGN-encapsulated albumin nanoparticles were prepared using a method modified from Ali Jahanban-Esfahlan et al. [30]. Briefly, 1.5 mg of KGN (BIDE, BD247584) was dissolved in 0.2 mL of DMSO and subsequently diluted in 5 mL of acetone. This acetone-DMSO solution of KGN was added dropwise to a bovine serum albumin (BSA) solution (40 mg of BSA in 2 mL of water, pH: 8.5), where 5 μmol of 1-ethyl-3-(-3-dimethylaminopropyl) carbodiimide hydrochloride (EDC) was subsequently added. The solution was stirred at room temperature for 3 h and centrifuged at 5000 RCF for 5 min. The supernatant was purified through an ultrafiltration tube with a molecular-weight cutoff (MWCO) of 50 kDa. The purified nanoparticles were collected and resuspended with sonication to obtain KGN-An stock solutions. The CHP peptide was coupled with KGN-An by a copper-free click reaction. After the quantification of albumin by BCA assay, the reaction was carried out (molar equivalent: albumin: DBCO-Sulfo-NHS ester: N_3–CHP = 1:5:5). Five equivalents of DBCO-Sulfo-NHS ester (Click Chemistry Tools, A124-100, 10 mM in PBS) were added into a solution of KGN-An (one equivalent of albumin in 0.8 mL of PBS) and mixed at room temperature for 1 h. The unreacted DBCO-Sulfo-NHS ester was removed through ultrafiltration. A PBS solution of N_3–CHP [0.8 μmol in 0.36 mL, custom synthesized, sequence: Ac–K(N_3)-Ahx-$(GfO)_9$, f: *cis*-4-fluoro-Pro] was then added for coupling with agitation overnight. Unreacted N_3–CHP was removed through centrifugation using an ultrafiltration tube (MWCO: 50 kDa).

The size distribution and Zeta potential of the KGN-An particles were examined through Dynamic Light Scattering (DLS) using a Zetasizer Nano instrument (Malvern, Zetasizer Nano). The BSA concentration was measured using a Bicinchoninic Acid Assay (BCA). The concentration of KGN in a solution of KGN-An was calculated using a UV absorbance measurement (285 nm) from a NanoPhotometer according to a predetermined standard curve. The encapsulation efficiency is given by

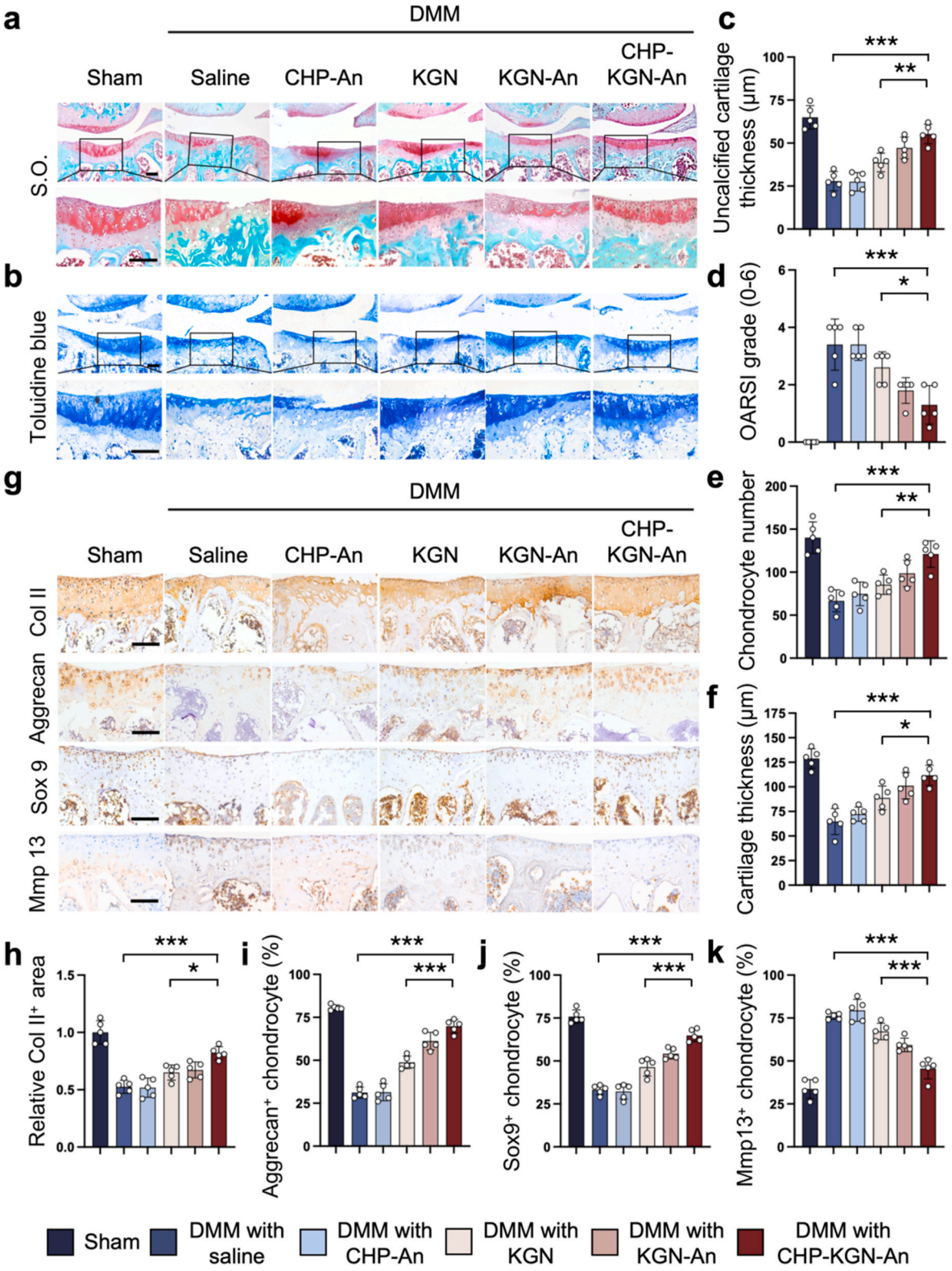

Fig. 4. CHP-KGN-An increased the KGN's protection against cartilage degeneration in the DMM mice (n = 5). (a) The representative Safranin-O/fast green staining of the mouse cartilage. (b) The representative toluidine blue staining of the mouse cartilage. (c) The quantification of the Safranin-O/fast green staining in terms of the uncalcified cartilage thickness. (d) The OARSI scores showing the extent of cartilage degradation in each treatment group. (e, f) The number of chondrocytes and full cartilage thickness quantified from the Safranin-O/fast green staining. (g) The representative IHC staining for Col II, Aggrecan, Sox9, and Mmp13 in the cartilage of mice by DMM or sham surgery. (h) The quantification of the Col II^+ area in the cartilage surface as shown by IHC staining. (i) The quantification of $Aggrecan^+$ chondrocyte population in the cartilage surface from the IHC staining. (j) The quantification of Sox 9^+ chondrocyte percentage in the cartilage surface from the IHC staining. (k) The quantification of $Mmp13^+$ chondrocyte percentage in the cartilage surface from the IHC staining. Scale bars, 100 μm (a, b), 50 μm (g). Data are shown as mean ± SD and analyzed using One-way ANOVA with Tukey's post-hoc test (c, e, f, h, i, j, k) or Kruska-Wallis test (d). $^*P < 0.05$; $^{**}P < 0.01$; $^{***}P < 0.001$.

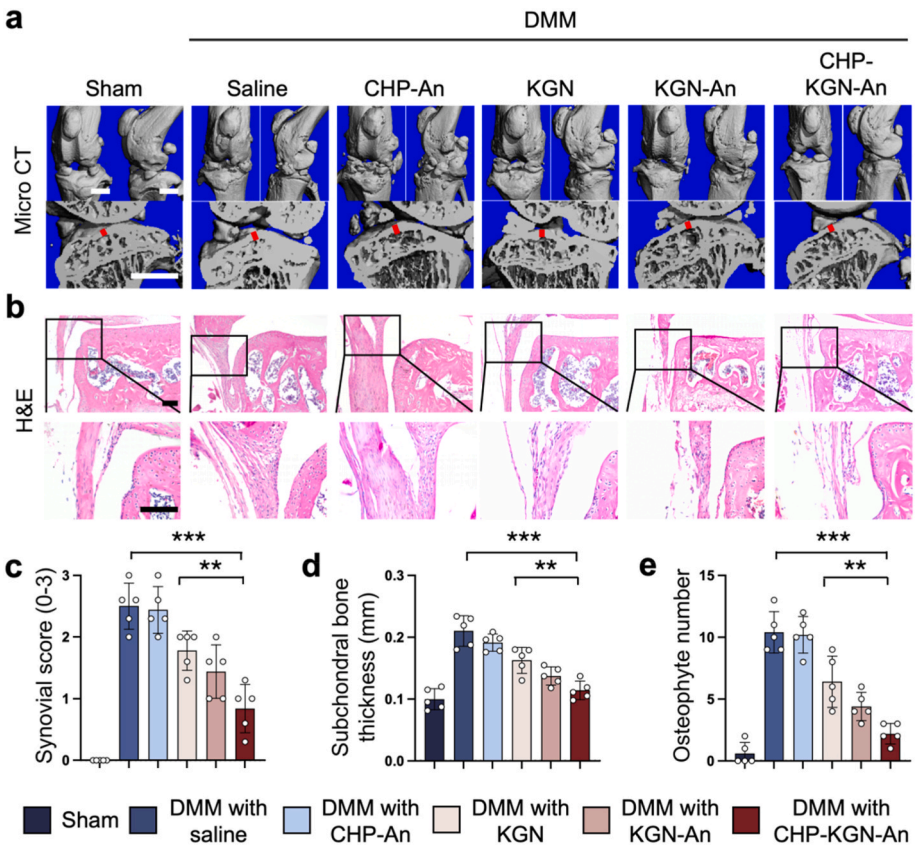

Fig. 5. CHP-KGN-An further attenuated bone remodeling and synovitis in the DMM mice compared with KGN (n = 5). (a) Representative reconstructed 3D micro-CT images of the mouse knee joints showed the osteophytes around the knee joints. The sagittal images of the medial tibial plateau demonstrated subchondral osteosclerosis. The red line marked the subchondral bone thickness. (b) Representative H&E staining of the mouse knee joints. (c) The quantification of the synovial score. (d) The quantification of subchondral bone thickness. (e) The quantification of the osteophyte number. Scale bars, 1 mm (a), 100 μm (b). Data are shown as mean ± SD and analyzed using one-way ANOVA with Tukey's post-hoc test (d, e) or Kruska-Wallis test (c). $^{**}P < 0.01$; $^{***}P < 0.001$.

w/W (%), and the amount of An-loaded KGN is termed as *w* while the total amount of drug added during the preparation process is *W*. To estimate the KGN release rate in vitro, a solution of CHP-KGN-An (1 mg of KGN in 1 mL) was dialyzed against 180 mL of blank PBS solution at 37 °C and sampled every 24 h to observe the optical quantification of the KGN concentration.

4.2. Ethics approval and consent to participate

All experimental animals and related experiments were authorized and carried out in full compliance with the regulations of the Animal Care and Use Committee of the Drum Tower Hospital Affiliated with the Nanjing University School of Medicine (2020AE01102), as well as the Experimental Animal Ethics Committee of the Fifth Affiliated Hospital of Sun Yat-sen University (approval no. 00059).

4.3. OA model

Twelve-week-old C57BL/6 mice were anesthetized using isoflurane. The skin surrounding the right knee joint was prepped and disinfected with a povidone-iodine solution. A surgical incision along the medial edge of the patellar ligament under a stereomicroscope, which revealed the medial compartment of the joint. The ligamentous attachments between the anterior horn of the medial meniscus and the tibial plateau were severed using a scalpel. The removal of the medial meniscus was verified with microforceps. Subsequent closure was performed in layers for the joint capsule and skin. The procedure was limited to a joint capsule incision, omitting the separation of the medial meniscus in the sham operation group [40].

4.4. Animal study

All experimental animals are 12-week-old male C57BL/6 mice from the Nanjing University Model Animal Research Center. All the animals were humanely housed in pathogen-free rodent housing with a 12-h light and dark cycle, with adequate water and food.

Mice were randomly divided into 6 groups and received [1]: Sham surgery (intra-articular injection, 8 μL normal saline per time, once a week) [2]; DMM surgery (intra-articular injection, 8 μL normal saline per time, once a week) [3]; DMM with KGN (intra-articular injection, KGN 50 μM, 8 μL per time, once a week) [4]; DMM with CHP-KGN-An (intra-articular injection, KGN 50 μM, 8 μL per time, once a week) [5]; DMM with KGN-An (intra-articular injection, KGN 50 μM, 8 μL per time, once a week) [6]; DMM with CHP-An (intra-articular injection, contain the same An concentration as in CHP-KGN-An group, 8 μL per time, once a week) for 10 weeks. All mice were euthanized 10 weeks after DMM surgery, and heart, spleen, kidney, liver, lung, and surgical knee samples were collected.

4.5. Targeting validation

C57BL/6 mice were injected with CHP-KGN-An (KGN 50 μM, 100 μL) 4 weeks after DMM surgery via tail-vein using an insulin needle. The in vivo fluorescence imaging was performed 5 h post-injection. The knee joint specimens were isolated for ex vivo fluorescence imaging. The IVIS imaging parameters: excitation/emission = 620/670 nm; pixel, 4; exposure, 1 s. For local delivery, mice were injected intra-articularly with Cy5-CHP-KGN-An or Cy5-^{S}CHP-KGN-An (^{S}CHP sequence: OfG-GOfGfGfOfOGOfGOOfGGOOffG) (KGN 50 μM, 8 μL) 5 h before

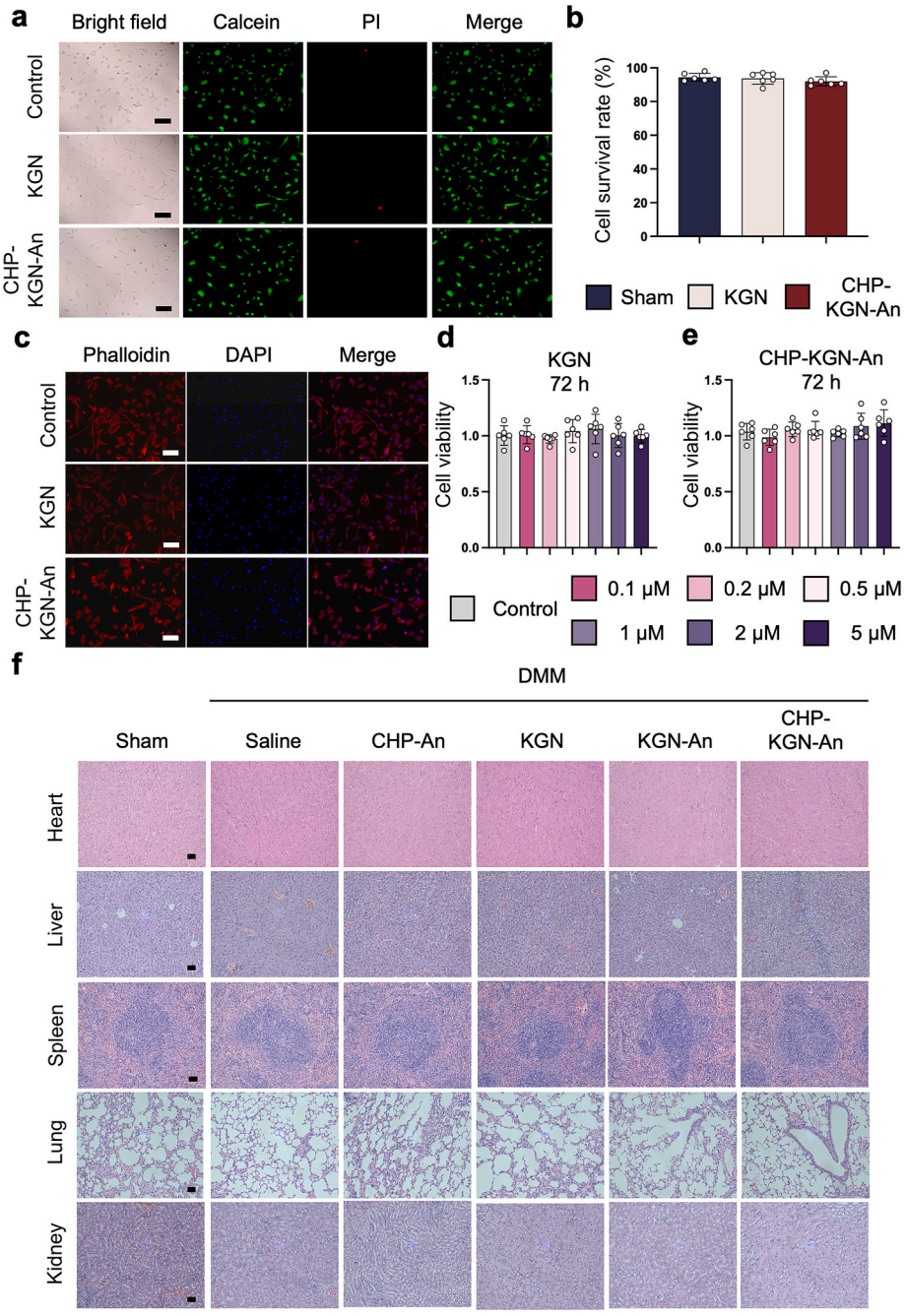

Fig. 6. In vivo and in vitro biocompatibility evaluation of CHP-KGN-An. (a) Representative Calcein-AM/PI staining of chondrocytes after incubating with 5 μM KGN or CHP-KGN-An capable of releasing equivalent dose of KGN within one day (n = 6 independent experiments). (b) The quantification of cell survival rate based on Calcein-AM/PI staining. (c) The representative phalloidin showing the chondrocyte morphology after incubating with 5 μM KGN or CHP-KGN-An capable of releasing the same dose of KGN within one day (n = 6 independent experiments). (d,e) CCK-8 assay for the viability of chondrocytes treated for with 100 nM to 5 μM KGN (d, 200 μL) or CHP-KGN-An capable of releasing 100 nM to 5 μM (200 μL) KGN (e) for 72 h. (f) Representative H&E staining of DMM mice's spleen, heart, lung, liver, and kidney. Scale bars, 100 μm (a,c), 50 μm (f). Data are shown as mean ± SD and analyzed using one-way ANOVA with Tukey's post-hoc test.

euthanasia and surgical isolation of the knee joint specimens. The knee joints were frozen in an OCT compound after standard procedures of paraformaldehyde fixation and EDTA decalcification. The articular cartilage was cryosectioned to observe the distribution of fluorescence intensity from Cy5-labeled CHP-KGN-An or ^{S}CHP-KGN-An. Tissue sections were imaged using an EVOS M7000 imaging system with an objective of 20 × and a light cube for Cy5 fluorescence.

4.6. Open field test (OFT)

Experimental mice were placed in an open-field apparatus measuring 50 cm × 50 cm respectively, with environmental brightness separately controlled to establish a controlled setting. A videographic system for real-time tracking was employed. Quantitative evaluations included activity, cumulative distance, duration of motion, and mean velocity [41].

4.7. Footprint assay

The mice's paws were color-coded with harmless dyes - forepaws with red and hind paws with black. Mice were allowed to ambulate along a 70 cm × 20 cm track lined with white paper under serene and dark conditions. The assay was conducted in triplicate for each mouse. The resulting paw prints served as a reflection of locomotor function and nociceptive thresholds. A habituation period of seven days preceded the testing to reduce environmental stressors [42].

4.8. Von Frey fiber test

Following a 30-min acclimatization in 7 cm × 7 cm × 7 cm enclosures, a Von Frey fiber device (38450, Ugo Basile, Italy) was applied to the plantar of the right hind limb to ascertain the mechanical threshold eliciting a paw withdrawal reflex. The experiment was executed by an operator blinded to the animal grouping to control for bias. A reduction in the withdrawal reflex threshold indicates heightened pain sensitivity [43].

4.9. Immunohistochemical (IHC) staining

Initial processing of surgical knee joint slices involved sequential hydration from xylene to graded ethyl alcohol solutions. Antigen repair employed pepsin at 37 °C for 1 h to unmask epitopes, followed by a 3 % hydrogen peroxide treatment to lessen endogenous peroxidase activity in a light-protected environment. After PBS washes, slices were blocked with 5 % BSA to reduce nonspecific binding and then incubated with primary antibodies targeting Mmp13 (#GB11247, Servicebio, China), Col II (#BA0533, Boster, China), Aggrecan (#13880-1-AP, Proteintech, China), Adamts5 (ab231595, abcam, England) and Sox9 (#67439-1-Ig, Proteintech, China) at 4 °C overnight. On day 2, slices were incubated with a secondary antibody which couples the Horseradish Peroxidase (HRP) for 1 h at room temperature. Development of color was produced with Ultra-Sensitive DAB Kit (#1205250, Typing), and cell nuclei were stained with hematoxylin.

4.10. Micro-CT evaluation

Micro-CT (VivaCT 80 scanner, Scanco Medical AG, Switzerland) was utilized to scan osteal structures of mice joints. Subchondral bone thickness and osteophyte numbers were calculated using Scanco Medical's three-dimensional reconstruction software [3].

4.11. Histological analysis

Decalcification of joint specimens was achieved over 4 weeks with a 10 % EDTA solution (#1340, Biofroxx). Specimen processing included dehydration in graded ethyl alcohol solutions and xylene, followed by paraffin embedding. Consistent 5 μm slices were generated with a microtome (Thermo Fisher Scientific, Germany) and stained with H&E (#C0105M, Beyotime, China), Safranin-O/fast green (#G1371, Solarbio, China), and Toluidine Blue (#G2543, Solarbio, China). Blind assessment using the Osteoarthritis Research Society International (OARSI) scoring system (scale 0–6) and synovitis score (scale 0–3) was implemented to appraise cartilage integrity and synovitis [44].

4.12. Cell viability

Cell counting kit-8 (CCK8) assays (Dojindo, Japan) were utilized to test cell viability. Chondrocytes were seeded in a 96-well plate at a density of 1×10^3 cells per well. KGN ranging from 100 nM to 5 μM and CHP-KGN-An releasing equivalent doses of KGN within 72 h were subsequently added to the cell culture medium. CCK8 experiments were performed at 24 h intervals after administration. We added 10 % CCK8 solution to each well, and the plates were incubated at 37 °C for 1 h. The optical density at 450 nm was then measured using a spectrophotometer [41].

4.13. Phalloidin staining

First-generation chondrocytes were seeded in a 6-well plate at a density of 2×10^4 cells. Once the cells reached 70 % confluence in the incubator, KGN and CHP-KGN-An were added and incubated for 24 h. After PBS washing, cells were fixed with 4 % paraformaldehyde for 15 min at room temperature. Following an additional PBS wash, the cells were incubated in a dark environment with Actin-Tracker Green-488 (Beyotime, China) for 30 min. After removing Actin-Tracker Green-488, the cells were stained with DAPI. Six hours later, cells were observed with a fluorescence microscope [45].

4.14. Calcein-AM/PI staining

The Calcein-AM/PI staining procedure was the same as phalloidin staining until the initial PBS wash. A prepared Calcein-AM/PI staining solution (Beyotime, China) was then added and incubated with first-generation chondrocytes for 30 min, followed by observation of living cells with a fluorescence microscope [46].

4.15. Statistical analysis

Quantitative data were derived from at least three independent specimens or sample replicates. The data were evaluated with the Shapiro-Wilk normality test and the Levene variance homogeneity test. A paired two-tailed student's t-test was used to compare the mean values between the two groups. A one-way ANOVA with Tukey's multiple comparison test was used for multiple-group comparisons. A Kruska-Wallis test was used for the comparison of OARSI score and synovitis score. Statistical analysis and data representations were processed through GraphPad Prism (version 9.0). Data were presented as mean ± standard deviation (SD), with statistical significance at $P < 0.05$ ($^*P < 0.05$; $^{**}P < 0.01$; $^{***}P < 0.001$).

CRediT authorship contribution statement

Yuxiang Fei: Writing – review & editing, Writing – original draft, Supervision, Project administration, Methodology, Investigation, Formal analysis, Data curation, Conceptualization. **Xiaojing Li:** Writing – review & editing, Writing – original draft, Validation, Methodology, Investigation, Data curation, Conceptualization. **Zhongyang Lv:** Writing – review & editing, Writing – original draft, Resources, Methodology, Data curation, Conceptualization. **Zizheng Liu:** Resources, Methodology, Investigation, Data curation. **Ya Xie:** Validation, Resources, Methodology, Data curation. **Jiaqi Chen:** Validation, Methodology, Investigation, Data curation. **Weitong Li:** Resources, Formal analysis, Data curation. **Xiyu Liu:** Methodology, Formal analysis, Data curation. **Hu Guo:** Project administration, Methodology, Investigation. **Huan Liu:** Validation, Software, Investigation. **Zhaofeng Zhang:** Supervision, Methodology, Data curation. **Xunhao Wang:** Methodology, Investigation. **Jingjing Fan:** Validation, Investigation. **Chunqing Hu:** Data curation. **Xiaoyu Jin:** Investigation. **Ruiyang Jiang:** Methodology. **Nuo Xu:** Data curation, Resources. **Jiang Xia:** Methodology, Resources. **Yang Li:** Writing – review & editing, Writing – original draft, Visualization, Validation, Software, Resources, Project administration, Methodology, Funding acquisition, Formal analysis, Data curation, Conceptualization. **Dongquan Shi:** Validation, Supervision, Project administration, Methodology, Conceptualization.

Declaration of competing interest

The authors declare that they have no known competing financial interests or personal relationships that could have appeared to influence

the work reported in this paper.

Acknowledgements

This work was supported by the National Natural Science Foundation of China (82325035, 82172481, 32271409, 82071977, and 92059104), the Six Talent Peaks Project of Jiangsu Province (WSW-079), the 2018 High-Level Health Team of Zhuhai, the Innovation Project of National Orthopedics and Sports Medicine Rehabilitation Clinical Medical Research Center (2021-NCRC-CXJJ-ZH-16), and the Guangdong-Hong Kong-Macao University Joint Laboratory of Interventional Medicine Foundation of Guangdong Province (2023LSYS001). Fig. 1a was created by Biorender.com.

Appendix A. Supplementary data

Supplementary data to this article can be found online at https://doi.org/10.1016/j.bioactmat.2024.08.004.

References

[1] D.J. Hunter, S. Bierma-Zeinstra, Osteoarthritis. Lancet 393 (10182) (2019) 1745–1759.
[2] A. Mahmoudian, L.S. Lohmander, A. Mobasheri, M. Englund, F.P. Luyten, Early-stage symptomatic osteoarthritis of the knee - time for action, Nat. Rev. Rheumatol. 17 (10) (2021) 621–632.
[3] Z. Lv, J. Han, J. Li, H. Guo, Y. Fei, Z. Sun, et al., Single cell RNA-seq analysis identifies ferroptotic chondrocyte cluster and reveals TRPV1 as an anti-ferroptotic target in osteoarthritis, EBioMedicine 84 (2022) 104258.
[4] J.N. Katz, K.R. Arant, R.F. Loeser, Diagnosis and treatment of hip and knee osteoarthritis: a review, JAMA 325 (6) (2021) 568–578.
[5] R. Deng, R. Zhao, Z. Zhang, Y. Chen, M. Yang, Y. Lin, et al., Chondrocyte membrane-coated nanoparticles promote drug retention and halt cartilage damage in rat and canine osteoarthritis, Sci. Transl. Med. 16 (735) (2024) eadh9751.
[6] I.A. Jones, R. Togashi, M.L. Wilson, N. Heckmann, C.T. Vangsness, Intra-articular treatment options for knee osteoarthritis, Nat. Rev. Rheumatol. 15 (2) (2019) 77–90.
[7] C. Larsen, J. Ostergaard, S.W. Larsen, H. Jensen, S. Jacobsen, C. Lindegaard, et al., Intra-articular depot formulation principles: role in the management of postoperative pain and arthritic disorders, J. Pharmaceut. Sci. 97 (11) (2008) 4622–4654.
[8] Z. Lv, P. Wang, W. Li, Y. Xie, W. Sun, X. Jin, et al., Bifunctional TRPV1 Targeted Magnetothermal Switch to Attenuate Osteoarthritis Progression, vol. 7, Research (Wash D C), 2024, p. 316.
[9] C. Shen, M. Gao, H. Chen, Y. Zhan, Q. Lan, Z. Li, et al., Reactive oxygen species (ROS)-responsive nanoprobe for bioimaging and targeting therapy of osteoarthritis, J. Nanobiotechnol. 19 (1) (2021) 395.
[10] N. Joshi, J. Yan, S. Levy, S. Bhagchandani, K.V. Slaughter, N.E. Sherman, et al., Towards an arthritis flare-responsive drug delivery system, Nat. Commun. 9 (1) (2018) 1275.
[11] M. He, Z. Qin, X. Liang, X. He, B. Zhu, Z. Lu, et al., A pH-responsive mesoporous silica nanoparticles-based drug delivery system with controlled release of andrographolide for OA treatment, Regen Biomater 8 (4) (2021) rbab020.
[12] Z. Ouyang, T. Tan, C. Liu, J. Duan, W. Wang, X. Guo, et al., Targeted delivery of hesperetin to cartilage attenuates osteoarthritis by bimodal imaging with Gd2(CO3)3@PDA nanoparticles via TLR-2/NF-κB/Akt signaling, Biomaterials 205 (2019) 50–63.
[13] S.K. Bedingfield, F. Yu, D.D. Liu, M.A. Jackson, C.L. Duvall, Matrix-targeted Nanoparticles for MMP13 RNA Interference Blocks Post-Traumatic Osteoarthritis, Cold Spring Harbor Laboratory, 2020.
[14] J. Martelpelletier, A.J. Barr, F.M. Cicuttini, P.G. Conaghan, C. Cooper, M. B. Goldring, et al., Osteoarthritis, Nat. Rev. Dis. Prim. 85 (1) (2016) 84.
[15] Z. Lv, Y.X. Yang, J. Li, Y. Fei, H. Guo, Z. Sun, et al., Molecular classification of knee osteoarthritis, Front. Cell Dev. Biol. 9 (2021) 725568.
[16] B. Brodsky, J.A. Ramshaw, The collagen triple-helix structure, Matrix Biol. 15 (8–9) (1997) 545–554.
[17] M.W. Kirkness, K. Lehmann, N.R. Forde, Mechanics and structural stability of the collagen triple helix, Curr. Opin. Chem. Biol. 53 (2019).
[18] X. Li, Q. Zhang, S.M. Yu, Y. Li, The chemistry and biology of collagen hybridization, J. Am. Chem. Soc. 145 (20) (2023) 10901–10916.
[19] J. Hwang, Y. Huang, T.J. Burwell, N.C. Peterson, J. Connor, S.J. Weiss, et al., In situ imaging of tissue remodeling with collagen hybridizing peptides, ACS Nano 11 (10) (2017) 9825–9835.
[20] Y. Li, C.A. Foss, D.D. Summerfield, J.J. Doyle, C.M. Torok, H.C. Dietz, et al., Targeting collagen strands by photo-triggered triple-helix hybridization, Proc. Natl. Acad. Sci. U.S.A. 109 (37) (2012) 14767–14772.
[21] H. Wahyudi, A.A. Reynolds, Y. Li, S.C. Owen, S.M. Yu, Targeting collagen for diagnostic imaging and therapeutic delivery, J. Contr. Release 240 (2016) 323–331.
[22] K. Huang, R. Qiu, Y. Fang, D. Zhu, X. Li, Z. Lv, et al., Targeting molecular collagen defects from the initiation of knee osteoarthritis, medRxiv (2024). https://www.medrxiv.org/content/10.1101/2024.06.13.24308739v2.
[23] M. Hou, Y. Zhang, X. Zhou, T. Liu, H. Yang, X. Chen, et al., Kartogenin prevents cartilage degradation and alleviates osteoarthritis progression in mice via the miR-146a/NRF2 axis, Cell Death Dis. 12 (5) (2021) 483.
[24] K. Johnson, S. Zhu, M.S. Tremblay, J.N. Payette, J. Wang, L.C. Bouchez, et al., A stem cell-based approach to cartilage repair, Science 336 (6082) (2012) 717–721.
[25] Q. Hu, B. Ding, X. Yan, L. Peng, J. Duan, S. Yang, et al., Polyethylene glycol modified PAMAM dendrimer delivery of kartogenin to induce chondrogenic differentiation of mesenchymal stem cells, Nanomedicine 13 (7) (2017) 2189–2198.
[26] M. Demoor, D. Ollitrault, T. Gomez-Leduc, M. Bouyoucef, M. Hervieu, H. Fabre, et al., Cartilage tissue engineering: molecular control of chondrocyte differentiation for proper cartilage matrix reconstruction, Biochim. Biophys. Acta 1840 (8) (2014) 2414–2440.
[27] L. Pandolfi, S. Minardi, F. Taraballi, X. Liu, M. Ferrari, E. Tasciotti, Composite microsphere-functionalized scaffold for the controlled release of small molecules in tissue engineering, J. Tissue Eng. 7 (2016) 2041731415624668.
[28] C.T. Laurencin, K.M. Ashe, N. Henry, H.M. Kan, K.W.H. Lo, Delivery of small molecules for bone regenerative engineering: preclinical studies and potential clinical applications, Drug Discov. Today 19 (6) (2014) 794–800.
[29] W.J. Gradishar, Albumin-bound paclitaxel: a next-generation taxane, Expet Opin. Pharmacother. 7 (8) (2006) 1041–1053.
[30] A. Jahanban-Esfahlan, S. Dastmalchi, S. Davaran, A simple improved desolvation method for the rapid preparation of albumin nanoparticles, Int. J. Biol. Macromol. 91 (2016) 703–709.
[31] Y. Yang, X. Zhao, S. Wang, Y. Zhang, A. Yang, Y. Cheng, et al., Ultra-durable cell-free bioactive hydrogel with fast shape memory and on-demand drug release for cartilage regeneration, Nat. Commun. 14 (1) (2023) 7771.
[32] Y. Qi, D. Zhou, J.L. Kessler, R. Qiu, S.M. Yu, G. Li, et al., Terminal repeats impact collagen triple-helix stability through hydrogen bonding, Chem. Sci. 13 (42) (2022) 12567–12576.
[33] B.J. Bielajew, J.C. Hu, K.A. Athanasiou, Collagen: quantification, biomechanics, and role of minor subtypes in cartilage, Nat. Rev. Mater. 5 (10) (2020) 730–747.
[34] A.O. Elzoghby, W.M. Samy, N.A. Elgindy, Albumin-based nanoparticles as potential controlled release drug delivery systems, J. Contr. Release 157 (2) (2012) 168–182.
[35] L.L. Bennink, Y. Li, B. Kim, I.J. Shin, B.H. San, M. Zangari, et al., Visualizing collagen proteolysis by peptide hybridization: from 3D cell culture to in vivo imaging, Biomaterials 183 (2018) 67–76.
[36] R.X. Zhang, K. Ren, R. Dubner, Osteoarthritis pain mechanisms: basic studies in animal models, Osteoarthritis Cartilage 21 (9) (2013) 1308–1315.
[37] K. Kalo, D. Niederer, M. Schmitt, L. Vogt, Acute effects of a single bout of exercise therapy on knee acoustic emissions in patients with osteoarthritis: a double-blinded, randomized controlled crossover trial, BMC Muscoskel. Disord. 23 (1) (2022) 657.
[38] J.Y. Kwon, S.H. Lee, H.-S. Na, K. Jung, J. Choi, K.H. Cho, et al., Kartogenin inhibits pain behavior, chondrocyte inflammation, and attenuates osteoarthritis progression in mice through induction of IL-10, Sci. Rep. 8 (1) (2018) 13832.
[39] H. Liu, P. Liu, Kartogenin promotes the BMSCs chondrogenic differentiation in osteoarthritis by down-regulation of miR-145-5p targeting Smad4 pathway, Tissue Eng Regen Med 18 (6) (2021).
[40] S.S. Glasson, T.J. Blanchet, E.A. Morris, The surgical destabilization of the medial meniscus (DMM) model of osteoarthritis in the 129/SvEv mouse, Osteoarthritis Cartilage 15 (9) (2007) 1061–1069.
[41] W. Li, Z. Lv, P. Wang, Y. Xie, W. Sun, H. Guo, et al., Near infrared responsive gold nanorods attenuate osteoarthritis progression by targeting TRPV1, Adv. Sci. 11 (16) (2024) e2307683.
[42] E.S. Trevisan, C.C.S. Martignago, L. Assis, J.C. Tarocco, S. Salman, L. Dos Santos, et al., Effectiveness of led photobiomodulation therapy on treatment with knee osteoarthritis: a rat study, Am. J. Phys. Med. Rehabil. 99 (8) (2020) 725–732.
[43] M.J. Piel, J.S. Kroin, H.-J. Im, Assessment of knee joint pain in experimental rodent models of osteoarthritis, Methods Mol. Biol. 1226 (2015) 175–181.
[44] W.-S. Choi, G. Lee, W.-H. Song, J.-T. Koh, J. Yang, J.-S. Kwak, et al., The CH25H-CYP7B1-RORα axis of cholesterol metabolism regulates osteoarthritis, Nature 566 (7743) (2019) 254–258.
[45] Y. Jin, Z. Li, Y. Wu, H. Li, Z. Liu, L. Liu, et al., Aberrant fluid shear stress contributes to articular cartilage pathogenesis via epigenetic regulation of ZBTB20 by H3K4me3, J. Inflamm. Res. 14 (2021) 6067–6083.
[46] S. Lei, J. Zhang, N.T. Blum, M. Li, D.Y. Zhang, W. Yin, et al., In vivo three-dimensional multispectral photoacoustic imaging of dual enzyme-driven cyclic cascade reaction for tumor catalytic therapy, Nat. Commun. 13 (1) (2022) 1298.